ChemComm

Cite this: *Chem. Commun.*, 2012, **48**, 9492–9494

www.rsc.org/chemcomm

COMMUNICATION

Dual template synthesis of a highly mesoporous SSZ-13 zeolite with improved stability in the methanol-to-olefins reaction†

Leilei Wu, Volkan Degirmenci, Pieter C. M. M. Magusin, Bartłomiej M. Szyja and Emiel J. M. Hensen*

Received 4th June 2012, Accepted 19th July 2012
DOI: 10.1039/c2cc33994c

The dual template synthesis of zeolite SSZ-13 by use of trimethyl-adamantanammonium hydroxide and a diquaternary-ammonium mesoporogen induces considerable mesoporosity without impeding zeolite microporosity. The strongly improved accessibility of Brønsted sites in mesoporous SSZ-13 increases its stability during application as an acid catalyst in the methanol-to-olefins reaction.

Zeolites are microporous crystalline aluminosilicates, which are widely used in the petrochemical industry for acid-catalyzed reactions. The strong Brønsted acidity of zeolites resides in tetrahedral Al^{3+} substitutions in the microporous SiO_2 framework, their combination giving rise to size- and shape-selective acid catalysis. Zeolites are usually synthesized in the form of relatively large crystals, which may lead to mass transport limitations during catalytic reactions. Many synthesis strategies, therefore, deal with improving the accessibility of zeolites either by increasing the size of the micropores[1] or by decreasing the size of the crystalline zeolite domains. The former is especially relevant for the (hydro)-conversion of heavy feedstocks. Often, however, relatively small pores are essential to achieve desired activity and selectivity in reactions with hydrocarbons. In such cases, the diffusion lengths can be decreased either by synthesizing nanocrystals[2] or by introducing substantial mesoporosity in zeolite crystals during their hydrothermal synthesis step or by post-synthesis treatments.[3] Earlier, many attempts have been made to combine structure directing agents (SDAs) for zeolite growth with surfactants usually employed to synthesize ordered mesoporous silicas. At best, this approach resulted in intimate mixtures of small zeolite crystals and amorphous mesoporous silica, however, with little benefit for catalysis.[4] The problem can be overcome by the use of cationic polymers[5] or by using surfactants that are covalently attached to the crystallizing zeolite phase.[6]

Schuit Institute of Catalysis, Eindhoven University of Technology, P.O. Box 513, Eindhoven, The Netherlands. E-mail: e.j.m.hensen@tue.nl; Fax: +31 40-245-5054; Tel: +31 40-247-5178

† Electronic supplementary information (ESI) available: Experimental procedures, argon physisorption, XRD patterns, $^{29}Si\{^{1}H\}$ HETCOR MAS NMR spectra, TPO profiles, MD simulations results, TEM images, and the product distribution of MTO. See DOI: 10.1039/c2cc33994c

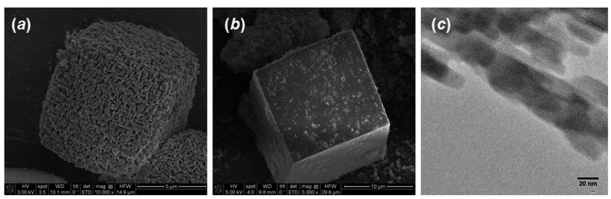

Fig. 1 SEM images of (a) mesoporous SSZ-13, (b) conventional SSZ-13 and (c) TEM image of mesoporous SSZ-13.

Herein, we report the first successful direct synthesis of a highly crystalline mesoporous SSZ-13 zeolite by combining two templates that are not grafted onto the zeolite. Mesoporous SSZ-13 was obtained *via* hydrothermal synthesis of a gel containing *N*,*N*,*N*-trimethyl-1-adamantanammonium hydroxide (TMAdOH) as the SDA and $C_{22}H_{45}$–$N^+(CH_3)_2$–$(CH_2)_4$–$N^+(CH_3)_2$–$C_4H_9Br_2$ ($C_{22\text{-}4\text{-}4}Br_2$) as the mesoporogen. Scanning electron microscopy (SEM) of mesoSSZ-13 (Fig. 1a) shows that the zeolite is obtained as a three-dimensional assembly of small nanocrystals intergrown into large micrometer-sized crystals. The more accessible texture of the mesoporous SSZ-13 is evident from a comparison to a SEM image of conventional SSZ-13 grown from a similar gel containing no $C_{22\text{-}4\text{-}4}Br_2$. The Si/Al ratios of mesoSSZ-13 and SSZ-13 are 17 and 19, respectively. By transmission electron microscopy (TEM, Fig. 1c), it is established that the extra pores in mesoSSZ-13 are not only in the macropore range, as Fig. 1a would suggest, but also in the mesopore range. This approach presents a generally applicable strategy for the synthesis of hierarchical zeolites involving the partial replacement of the conventional SDA by a mesoporogen.

SSZ-13 is a zeolite with the chabazite (CHA) topology. In its silicoaluminophosphate form (SAPO-34) it is the preferred catalyst for the methanol-to-olefins (MTO) process, which is an important step in the conversion of synthesis gas to polymer-grade olefins from methanol.[7] The reaction involves an organic reaction center, formed *in situ* in the large cavities of zeolite crystals.[8] Coke formation occurs preferentially in the near-surface region of the chabazite crystals.[9] The decreased accessibility of the micropore space leads to catalyst deactivation. To improve catalyst stability for the MTO reaction it is desirable to increase the ratio of external over internal surface area of the zeolite catalyst.[10] Desilication of SSZ-13 has been shown

to introduce mesoporosity, however, without benefit for the MTO reaction.[11]

In our dual template approach, we used TMAdOH as the SDA for chabazite growth.[12] For the mesoporogen, we took into account that it should contain (i) a hydrophobic tail to limit the crystal growth and (ii) a head group that has sufficient interaction with the growing zeolite phase. Compared to single quaternary ammonium head groups, SDAs with two ammonium head groups are effective for zeolite growth as shown by the group of Ryoo. Therefore, we explored the use of this type of surfactants to limit the size of the crystalline domains of SSZ-13. For example, by using surfactants of the type $R–N^+(CH_3)_2–(CH_2)_6–N^+(CH_3)_2–C_6H_{13}$ with R = alkyl chain as templates, Ryoo *et al.* synthesized sheet-like ZSM-5.[10] Similar approaches using a head group with a single quaternary ammonium center result in ordered mesoporous silicas of the M41S class.[13]

To guide the design of the mesoporogen we carried out a computational study to determine the best fit of three candidate surfactants, $C_{22}H_{45}–N^+(CH_3)_2–(CH_2)_4–N^+(CH_3)_2–C_4H_9$ ($C_{22\text{-}4\text{-}4}$), ($C_{22}H_{45}–N^+(CH_3)_2–(CH_2)_6–N^+(CH_3)_2–C_6H_{13}$) ($C_{22\text{-}6\text{-}6}$) and $C_{22}H_{45}–N^+(CH_3)_2–C_4H_9$ ($C_{22\text{-}4}$), in the growing CHA framework. The first one was chosen because tetraethylammonium is a known SDA for CHA.[14] By linking two such moieties with a hydrophobic tail, we expect significant interactions with SSZ-13 in analogy with the $C_{22\text{-}6\text{-}6}$ for ZSM-5.[10] A further comparison is made with $C_{22\text{-}4}$ to establish the effect of a single quaternary ammonium head group. We employ classical Molecular Dynamics (MD) simulations because they allow efficient sampling of phase space and take into account van der Waals interactions in contrast to DFT.[15] The all-silica CHA model contained 2 × 3 × 4 unit cells with one surface being terminated by silanol groups. In all cases, the zeolite contained TMAd cations and one mesoporogen. The template–framework interaction and framework destabilization energies are given in Table 1.

Fig. 2 shows the preferred configuration (I) of $C_{22\text{-}4\text{-}4}$ in SSZ-13 with one quaternary ammonium center in the cavity below the surface and the other one at the surface. The interaction energy (−247 kJ mol^{-1}) is higher than that of TMAd in SSZ-13 (−163 kJ mol^{-1}). This configuration is preferred over configuration II with both quaternary ammonium centers in the cavities below the surface (Fig. S5, ESI†), because the interaction energy (−242 kJ mol^{-1}) is lower than the configuration in which two TMAd templates occupy these cavities (−326 kJ mol^{-1}). Note that, in this case, one TMAd cation is placed outside the framework (Fig. S5, ESI†). $C_{22\text{-}6\text{-}6}$ adopts a similar configuration I, but the terminal hexyl fragment

Table 1 Interaction of candidate quaternary ammonium templates with the all-silica chabazite framework[a]

Mesoporogen	$C_{22\text{-}4\text{-}4}$	$C_{22\text{-}4\text{-}4}$	$C_{22\text{-}6\text{-}6}$	$C_{22\text{-}4}$
Configuration[b]	I	II	I	II
$\Delta E_{\text{framework–template}}$	−247	−242	−242	−155
$\Delta E_{\text{framework destabilization}}$	+28	+28	+39	+28

[a] Energies in kJ mol^{-1}. [b] Configuration I: one quaternary ammonium center at the surface, II: quaternary ammonium center(s) below the surface.

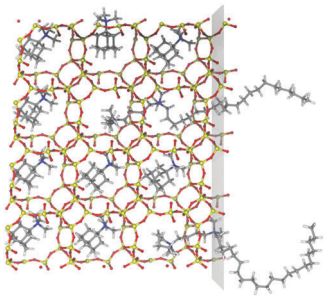

Fig. 2 Snapshot of a MD simulation of a $C_{22\text{-}4\text{-}4}$ cation interacting with the CHA framework in the presence of 3 TMAd cations, corresponding to configuration I (red: oxygen; yellow: silicon, gray: carbon, white: hydrogen; blue: nitrogen). The gray plane indicates the terminating zeolite surface.

is folded back in the large cavity, likely because of the repulsion with the TMAd in the adjacent cavity (Fig. S6, ESI†). This leads to stronger framework destabilization compared to $C_{22\text{-}4\text{-}4}$. With $C_{22\text{-}4}$ in configuration I the template became detached from the zeolite surface (Fig. S7, ESI†). In configuration II, the framework–template interaction energy is below that of TMAd. Based on these results, we predicted $C_{22\text{-}4\text{-}4}Br_2$ to be the preferred mesoporogen.

Crystallization of a gel containing only $C_{22\text{-}4\text{-}4}Br_2$ yielded an amorphous product. The XRD patterns of the products (Fig. S1, ESI†) obtained by combining TMAdOH and candidate mesoporogens are compared to the pattern of SSZ-13. The use of $C_{22\text{-}4\text{-}4}Br_2$ resulted in a crystalline zeolite with the CHA structure (Fig. S1b, ESI†). No competing crystalline phases were detected. The crystallinity of mesoporous SSZ-13 is 90%, comparable to that of conventional SSZ-13 (92%). Argon physisorption (Table S1, ESI†) evidenced the substantial mesoporosity of mesoporous SSZ-13 (V_{meso} = 0.21 cm^3 g^{-1}) as compared to conventional SSZ-13 (V_{meso} = 0.01 cm^3 g^{-1}). The micropore volumes are quite similar at 0.18 and 0.21 cm^3 g^{-1} for conventional and mesoporous SSZ-13, respectively. In accordance with Fig. 1, the mesopore size distribution of mesoporous SSZ-13 is quite broad.

Our MD simulations show that the role of $C_{22\text{-}4\text{-}4}$ is to inhibit crystal growth in the direction of the aliphatic chain. $^{29}Si\{^1H\}$ HETCOR MAS NMR of as-synthesized mesoporous SSZ-13 (Fig. S3, ESI†) shows the close proximity of the framework silicon atoms to the hydrogen atoms of TMAdOH and the $N–CH_{n=2,3}$ moieties in $C_{22\text{-}4\text{-}4}$, but not to the hydrogen atoms in the C_{22} chains. This indicates that the C_{22} chains are located outside the framework as predicted by the MD simulations. Because of the cubic symmetry of CHA, there is no preferred crystallographic direction in which the mesoporogen is oriented and, therefore, no sheet-like crystals are obtained in this case. As a consequence, SSZ-13 nanocrystals will form a wide range of cubic shapes.

To verify our prediction about $C_{22\text{-}4\text{-}4}$ as the preferred template for hierarchical SSZ-13, we synthesized SSZ-13 in the presence of $C_{22\text{-}6\text{-}6}$ and $C_{22\text{-}4}$ and obtained much less crystalline materials (68% and 13%, respectively). The material prepared in the presence of $C_{22\text{-}6\text{-}6}$ has a high mesopore volume (0.45 ml g^{-1}) with a substantial contribution of mesopores of around 3 nm. The lower micropore volume (0.10 ml g^{-1})

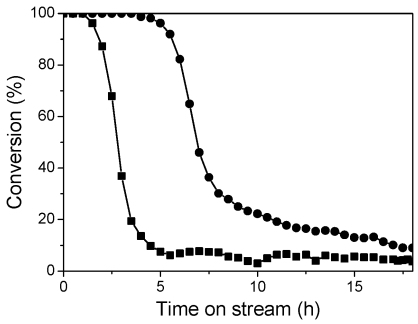

Fig. 3 Methanol conversion of (■) conventional SSZ-13 and (●) highly mesoporous SSZ-13 synthesized by use of our dual template approach (MTO, T = 350 °C; WHSV = 0.8 g g^{-1}).

correlates with the lower crystallinity. These results indicate that this sample is a mixture of an amorphous phase ordered at the mesoscale and a crystalline mesoporous SSZ-13 phase in agreement with TEM images of this sample (Fig. S8, ESI†).

A remarkable feature of our mesoporous SSZ-13 is its much improved stability in the MTO reaction compared to conventional SSZ-13 (Fig. 3). For both catalysts, the initial methanol conversion is 100%, indicating that mesoporous SSZ-13 contains similar strong Brønsted acid sites as SSZ-13. The lifetime (defined as the time to reach methanol conversion of 50%) increased from 2.8 h for SSZ-13 to 6.8 h for mesoporous SSZ-13. The product composition after 1 h time on stream is comparable for both catalysts with a combined ethylene and propylene selectivity higher than 90% (Table S2, ESI†). The improved catalyst stability is a result of a more efficient utilization of the zeolite micropore space. Deactivation of MTO catalysts is caused by pore blockage by carbonaceous deposits.[16] Spectroscopic imaging has shown that the larger carbonaceous deposits, which deactivate the catalyst, accumulate in the near-surface region of the crystals.[9] Accordingly, deactivation will depend on the surface to volume ratio of the crystals. Substantial mesoporosity as present in mesoporous SSZ-13 implies high external surface area and more efficient utilization of the micropore space. Analysis of the amount of coke by TPO of the spent catalysts (Fig. S4, ESI†) corroborates this interpretation: spent mesoSSZ-13 contains about twice the amount of coke (32 wt%) as conventional SSZ-13 (16 wt%).

In summary, we have shown that highly mesoporous SSZ-13 can be synthesized in a single step by combining an SDA for CHA formation with a diquaternary ammonium type surfactant. Predictive design of templates to generate desirable porous structures for catalysis remains a grand challenge.[17] In our case, computational modelling aided in the design of the mesoporogen, which interacts strongly enough with the growing zeolite framework and competes with the SDA so that the growth of the zeolite crystal is interrupted. This approach presents a generally applicable strategy for the synthesis of hierarchical zeolites, because it requires only to replace a small part of the conventional SDA by a usually more expensive mesoporogen. This is an advantage over approaches involving the single use of an expensive template, which combines zeolite directing and mesoporogen functions.[10] When applied to SSZ-13, a significantly more stable catalyst for the MTO reaction is obtained. The increase in catalyst longevity is directly related to the high interconnectivity of micro- and mesopores within the zeolite. The inhibition of the zeolite growth in all directions by the surfactant leads to cubic nanocrystals of CHA zeolites intergrown into larger structures.

Financial support from the Technology Foundation STW, the applied science division of the Netherlands Organization for Scientific Research (NWO) and the Programme Strategic Alliances between China and the Netherlands is acknowledged. We also thank the Soft Matter Cryo-TEM Research Unit of Eindhoven University of Technology.

Notes and references

1 A. Corma, M. J. Díaz-Cabaña, J. Martínez-Triguero, F. Rey and J. Rius, *Nature*, 2002, **418**, 514.
2 D. P. Serrano, J. Aguado, J. M. Escola, J. M. Rodriguez and A. Peral, *J. Mater. Chem.*, 2008, **18**, 4210.
3 (*a*) J. Pérez-Ramirez, C. H. Christensen, K. Egeblad, C. H. Christensen and J. C. Groen, *Chem. Soc. Rev.*, 2008, **37**, 2530; (*b*) R. Chal, C. Gerardin, M. Bulut and S. van Donk, *ChemCatChem*, 2011, **3**, 67.
4 (*a*) A. Karlsson, M. Stöcker and R. Schmidt, *Microporous Mesoporous Mater.*, 1999, **27**, 181; (*b*) L. M. Huang, W. P. Guo, P. Deng, Z. Y. Xue and Q. Z. Li, *J. Phys. Chem. B*, 2000, **104**, 2817.
5 (*a*) F. Liu, T. Willhammar, L. Wang, L. Zhu, Q. Sun, X. J. Meng, W. Carrillo-Cabrera, X. Zou and F.-S. Xiao, *J. Am. Chem. Soc.*, 2012, **134**, 4557; (*b*) F.-S. Xiao, L. Wang, C. Yin, K. Lin, Y. Di, J. Li, R. Xu, D. S. Su, R. Schlgl, T. Yokoi and T. Tatsumi, *Angew. Chem., Int. Ed.*, 2006, **45**, 3090.
6 (*a*) M. Choi, H. S. Cho, R. Srivastava, C. Venkatesan, D.-H. Choi and R. Ryoo, *Nat. Mater.*, 2006, **5**, 718; (*b*) A. Inayat, I. Knoke, E. Spiecker and W. Schwieger, *Angew. Chem., Int. Ed.*, 2012, **51**, 1962.
7 (*a*) J. F. Haw, W. Song, D. M. Marcus and J. B. Nicholas, *Acc. Chem. Res.*, 2003, **36**, 317; (*b*) S. Kvisle, T. Fuglerud, S. Kolboe, U. Olsbye, K. P. Lillerud and B. V. Vora, *Handbook of Heterogeneous Catalysis*, ed. H. Ertl, F. Knözinger, F. Schüth and J. Weitkamp, Wiley-VCH, Weinheim, 2nd edn, 2008, vol. 6, p. 2950.
8 (*a*) D. Lesthaeghe, B. De Sterck, V. Van Speybroeck, G. B. Marin and M. Waroquier, *Angew. Chem., Int. Ed.*, 2007, **46**, 1311; (*b*) D. M. McCann, D. Lesthaeghe, P. W. Kletnieks, D. R. Guenther, M. J. Hayman, V. van Speybroeck, M. Waroquier and J. F. Haw, *Angew. Chem., Int. Ed.*, 2008, **47**, 5179.
9 (*a*) D. Mores, E. Stavitski, M. H. F. Kox, J. Kornatowski, U. Olsbye and B. M. Weckhuysen, *Chem.–Eur. J.*, 2008, **14**, 11320; (*b*) D. Mores, J. Kornatowski, U. Olsbye and B. M. Weckhuysen, *Chem.–Eur. J.*, 2011, **17**, 2874.
10 M. Choi, K. Na, J. Kim, Y. Sakamoto, O. Terasaki and R. Ryoo, *Nature*, 2009, **461**, 246.
11 L. Sommer, D. Mores, S. Svelle, M. Stöcker, B. M. Weckhuysen and U. Olsbye, *Microporous Mesoporous Mater.*, 2010, **132**, 384.
12 L. T. Yuen, S. I. Zones, T. V. Harris, E. J. Gallegos and A. Auroux, *Microporous Mater.*, 1994, **2**, 105.
13 C. T. Kresge, M. E. Leonowicz, W. J. Roth, J. C. Vartuli and J. S. Beck, *Nature*, 1992, **359**, 710.
14 B. M. Lok, C. A. Messina, R. L. Patton, R. T. Gajek, T. R. Cannan and E. M. Flanigen, *US Patent*, 4440871, 1984.
15 B. Smit and T. L. M. Maesen, *Nature*, 2008, **451**, 671.
16 D. M. Bibby, R. F. Howe and G. D. McLellan, *Appl. Catal., A*, 1992, **93**, 1.
17 (*a*) D. W. Lewis, C. R. A. Catlow, J. M. Thomas, D. J. Willock and G. J. Hutchings, *Nature*, 1996, **382**, 604; (*b*) S. M. Woodley and R. Catlow, *Nat. Mater.*, 2008, **7**, 937.

